Enhanced Light Trapping in GaAs/TiO2-Based Photocathodes for Hydrogen Production

Thomas Dursap, Mariam Fadel, Philippe Regreny, Cristina Tapia Garcia, Céline Chevalier, Hai Son Nguyen, Emmanuel Drouard, Solène Brottet, Michel Gendry, Alexandre Danescu, et al.

Enhanced light trapping in GaAs / TiO_2 based photocathodes for hydrogen production

Thomas Dursap[1], Mariam Fadel[2], Philippe Regreny[1], Cristina Tapia Garcia[2], Céline Chevalier[1], Hai Son Nguyen[1], Emmanuel Drouard[1], Solène Brottet[1], Michel Gendry[1], Alexandru Danescu[1], Matthieu Koepf[2,], Vincent Artero[2], Matthieu Bugnet[3,*], José Penuelas[1,*]*

1 Univ. Lyon, CNRS, ECL, INSA Lyon, UCBL, CPE Lyon, INL, UMR 5270, 69130 Ecully, France

2 Univ. Grenoble Alpes, CNRS, CEA, IRIG, Laboratoire de Chimie et Biologie des Métaux, 38000 Grenoble, France

3 Univ. Lyon, CNRS, INSA Lyon, UCBL, MATEIS, UMR 5510, 69621 Villeurbanne, France

ABSTRACT. Photoelectrochemical cells (PEC) are appealing devices for the production of renewable energy carriers. In this context, III-V semiconductors such as GaAs are very promising materials due to their tunable bandgaps, which can be appropriately adjusted for sunlight harvesting. Because of the high cost of these semiconductors, the nanostructuration of the photoactive layer can help to improve the device efficiency as well as drastically reduce the amount of material needed. III-V nanowire-based photoelectrodes benefit from the intrinsically high aspect ratio of nanowires, their enhanced ability to trap light as well as their improved charge separation

and collection abilities, and thus are particularly attractive for PECs. However, III-V semiconductors often suffer from corrosion in aqueous electrolytes, preventing their utilization over long periods under relevant working conditions. Here, photocathodes of GaAs nanowires protected with thin TiO_2 shells were prepared and studied under simulated sunlight irradiation to assess their photoelectrochemical performances in correlation with their structural degradation, highlighting the advantageous nanowire geometry compared to its thin film counterpart. Morphological and electronic parameters, such as the aspect-ratio of the nanowires and their doping pattern were found to strongly influence the photocatalytic performances of the system. This work highlights the advantageous combination of nanowires featuring a buried radial p-n junction with Co-nanoparticles used as hydrogen evolution catalyst. The nanostructured photocathodes exhibit significant photocatalytic activities, comparable with previous noble-metal based systems. This study demonstrates the potential of GaAs nanostructured semiconductor and its reliable use for photo-driven hydrogen production.

KEYWORDS. hydrogen evolution reaction, photocathode, GaAs, nanowires, cobalt catalyst

Introduction

Concomitantly to the development of industrialized societies, the use of fossil fuels such as natural gas, oil, and coal as primary energy sources has drastically increased since the beginning of last century[1] leading to the release of ever-larger quantities of CO_2, which are at the origin of the current global warming effect. The search for alternative strategies to provide energy at a large scale with a lower carbon-footprint has become a critical issue for the scientific community. Among all devices with high potential of applicability, intense efforts are carried out for the development of photoelectrochemical cells (PEC). Following the basic principles of photosynthesis, these devices are able to harvest and use solar energy to drive specific chemical reactions, and convert abundant resources (H_2O, CO_2, N_2, etc.) into energy-rich compounds (H_2, CH_3OH, NH_3, etc.) that are stable, can be stored, and are easily distributed[2,3]. In this context, solar-driven water splitting is a major target as it involves rather simple chemical reactions and water, which is a widespread and easy-to-handle reagent[4]. Electrochemical devices for water splitting typically combine an anode material (or combination of materials) where water is oxidized to O_2 through the oxygen evolution reaction (OER), and a cathode material (or combination of materials) where protons are reduced to H_2 through the hydrogen evolution reaction (HER). In the case of PEC, at least one of the two electrode materials must be able to absorb sunlight to generate the electrochemical potential required to drive the OER and HER reactions[5]. TiO_2 has been the first effective photoanode material reported for water splitting, in 1972, by A. Fujishima and K. Honda[6]. This pioneering study triggered intense efforts by the scientific community to improve the efficiency of the solar-to-hydrogen (STH) conversion[7]. However, despite being a cheap and robust material for the design of photoanodes, the large bandgap of TiO_2 (~3.2 eV) restricts its absorption to a very small fraction of the solar spectrum ($\lambda_{abs} < 400$ nm), strongly limiting the maximum STH

efficiency reachable with devices based only on this oxide[8]. In the quest for alternative solutions, III-V semiconductors (SCs) such as GaAs emerged as advantageous material constituents of photoelectrodes due to their narrower bandgap (1.4 eV in the case of GaAs) and adequately positioned valence band, allowing for the use of a substantially larger portion of the solar spectrum to drive the OER and HER reactions[5,9,10]. Thus, III-V SCs have attracted a fair amount of attention for solar fuels applications.

Besides the choice of the SC material implemented within PEC devices, the control of the morphology of the electrodes was recently recognized as a critical factor controlling both the light absorption properties as well as the efficiency of the electrochemical reaction occurring at the interface with the electrolyte[11]. III-V nanowires (NWs) present a high aspect-ratio improving their light-trapping efficiency and have a strong ability to be grown on low-cost silicon substrate, making them particularly attractive to design innovative photoelectrodes for light-driven water splitting[12]. While many studies have been focusing on the use of III-V NWs as photoanodes for the OER, only few reports are available on the use of these materials as photocathodes for the HER[13–15]. A recent work by Zhou *et al.* indicated a significant enhancement of the STH efficiency, reaching performances close to 10% using the GaP NW combined with a complex heterostructure and bandgap engineering[15]. If the corrosion of these materials has limited the viability of their use in actual devices thus far, Cui *et al.* recently demonstrated the possibility to overcome this issue by protecting the surface of the nanowires with a thin TiO_2 oxide layer[14]. While this latter study suggests that III-V NW-based photoelectrodes could still be used for solar fuel production, the current state-of-the-art also shows that several open questions remain to be answered. For instance, the influence of morphological parameters of the nanowires such as their aspect-ratio, and their crystallinity or verticality on the PEC performance is seldom investigated. Additionally, the influence of the doping profile of the semiconductor, such as a p-n junction, remains unexplored.

The use of non-noble metal catalysts, instead of commonly used Pt[14], is also a meaningful approach for cost-reduction and use of abundant resources that should be privileged[16]. Furthermore, the TiO_2 protective layer quality could possibly introduce variations of the PEC efficiency. Therefore, it appears necessary to study these different pathways with the aim to further optimize the efficiency of PEC cathode components for HER.

In this work, the influence of the NW geometry on the photocathode efficiency is investigated by comparing the photocurrent generated by a 2D GaAs thin film, and by self-assisted GaAs NWs protected with a thin TiO_2 shell, both grown on low-cost silicon (111) substrates by molecular beam epitaxy. After confirming the benefit of using a nanostructured electrode compared to flat GaAs substrate, the performances of photoelectrodes featuring different NW morphologies are systematically evaluated. For the best architecture, the benefit of including a buried p-n junction within NWs is studied. Finally a Co-based catalyst is integrated at the surface of the NWs, which leads to photocathodes exhibiting comparable photocurrent densities as Pt-decorated TiO_2-protected electrodes previously reported in literature[14]. A schematic illustrating the different steps leading to the final nanostructures is shown in Figure 1 This study demonstrates that finely tuning the NW morphology and doping profile provides efficient photocathodes for HER at neutral pH without the need of using a noble metal catalyst.

Results and discussion

Geometry

In order to evaluate the influence of the geometry of the active material on the photocurrent density generated under irradiation, a thin 2D layer of B-doped GaAs and a sample of self-assisted B-doped GaAs NWs were deposited on separate p-doped silicon substrates. Details of the growth are available in Methods. The NWs were ~2.3 ± 0.3 μm long, for a mean diameter of 125 ± 20 nm,

reaching a density of around 1.1 NWs/µm². The total volume of GaAs deposited during the NWs growth hence corresponds to 3.1 x 10^{-6} cm^3 for an effective surface, *i. e.* the surface in contact with the electrolyte, of around 1.01 cm², which is equivalent to the effective surface of the GaAs thin film counterpart.

The samples were placed in 0.1 M potassium phosphate buffer (pH 7) and linear sweep voltammograms (LSV) were recorded under chopped-light irradiation using a Xe lamp equipped with an AM 1.5 filter (simulated 1 sun irradiation, 100 mW/cm²; see Methods for details). As shown in Figure 2.a, photocurrents were observed for both NW and thin film samples, although with distinct onset potentials and current densities. The NWs led to photocurrents with an onset potential of + 0.35 V vs RHE, while a lower onset potential of + 0.25 V vs RHE was observed in the case of the thin film indicating that the NWs are able to drive more efficiently (ie with higher photopotential) reductive processes under irradiation. Moreover, the NWs delivered significantly higher photocurrent than the thin film, with almost two to three times higher current recorded over the full range of the explored potentials, although the volume of the photoactive material (GaAs) deposited is ten times higher for the thin film. Since the geometric surface area for light collection of the two samples were both equal to ~1.0 cm², it is likely that the enhancement of the photocurrent is largely associated to the improved light-trapping efficiency of the NWs compared to the thin film. Indeed, as shown in Figure 2.b, the NW geometry induces a reduction of the reflectivity down to 2%, compared to around 30% for the thin film, indicating an enhancement of the sample light absorption efficiency, and thus demonstrating the strong potential of the nanostructuration of GaAs into NWs to design improved photoelectrodes for PEC applications. The NWs grown for this comparison are shown in Figure 3.a. Besides the light trapping effect, several other factors can influence the overall efficiency of charge carrier generation and collection upon nanostructuration of the absorbing material[17]. Additional experiments that are outside the scope of this study would,

however, be necessary to assess the contribution of each individual factors. In any case, our observations are in agreement with the observations performed by A. Javay's group[18] or E. P. A. M. Bakkers's group[19] on InP or GaP NWs, respectively, and C. Cornet's group[20] for GaAs/Si photoelectrodes.

Morphology

The impact of the morphology of these objects on the photocurrent density were further investigated under simulated 1 sun irradiation. Three NW samples were grown with different morphologies as illustrated in Figure 3.a-c, and described in Table 1. The different morphologies were obtained for different radial growth times (more details in Method section). Sample 1, shown in Figure 3.a, presents the largest aspect ratio (length/diameter) but the smallest effective surface area. Samples 2 and 3, corresponding to NWs after 1 hour and 2 hours of radial p-doped GaAs growth, respectively, are shown in Figure 3.b and Figure 3.c. By increasing the length and the diameter of the NWs (values reported in Table 1), the total effective surface area of GaAs materials exposed to the electrolyte increases, for a comparable NW density.

The sample bearing the shortest and thinnest NWs (Figure 3.a) delivers a photocurrent of around 0.10 mA/cm² at 0.0 V vs RHE, while a value close to 0.31 mA/cm² was obtained at 0.0 V vs RHE for the thickest NWs (Figure 3.c). The improvement of the photocurrent density can be attributed to the increase of the effective surface area of GaAs material in contact with the electrolyte (Figure 3.e), and to enhanced light trapping efficiency by the largest NWs as shown in Figure 3.f. The reflected light in the 350-850 nm spectral range drops from about 2% for the shortest and thinnest NWs (blue lines) to about 0.5% for the thickest ones (green lines). While the reflectance of the different samples was experimentally measured, it was not possible to obtain information on the absorptance of those samples. Finite difference time domain (FDTD)

simulations were used to further investigate on the optical properties of our samples, using ANSYS Lumerical FDTD solutions.

The simulated reflectance thus confirms the tendencies observed in the experiment (see Supporting Information for details). Simulations also show the contribution of the GaAs material and of the Si substrate on the light absorptance (see Supporting Information for details), confirming the optimal sample morphology.

p-n junction

In order to drive the targeted chemical reactions at the solid-liquid interface, efficient charge migration must occur from the core of the NWs to its surface. This phenomenon requires the establishment of an adequate gradient of potential between the bulk SC material, here GaAs, and the electrolyte. Ensuring that electrons reach the edge of the GaAs NWs should improve the overall efficiency of the photocathodes. For this purpose, an n-doped shell was grown using Si as dopant around the p-doped core NW, as illustrated in Figure 4.a, aiming for the same dimensions as the NWs of sample 3. The implementation of such p-n junction leads to band edge bending at the interface between the p-core and n-shell, as shown in Figure 4.b, which should favor the separation of the electron-hole pairs and reduce their recombination rate within the NWs. On the bare NWs (sample 3), the LSV measurements performed on samples featuring the buried p-n junction reveal an increase of the photocurrent density of about 30%, up to around 0.4 mA/cm² at 0 V vs RHE, compared to 0.3 mA/cm² for the monolithic p-doped NWs, as shown in Figure 4.c. Furthermore, another significant enhancement of the current density delivered by the samples featuring the NWs containing the p-n junction is observed after the integration of Co-based nanoparticles on the electrodes, a well-known catalyst for the hydrogen evolution reaction (HER)[21]. Indeed, after the photoassisted deposition of the nanoparticles (see the Methods for the experimental details), the

current density reaches up to 1.15 mA/cm² at 0 V *vs* RHE in neutral electrolyte (Figure 5.b and c). This contrasts with the samples based on monolithic p-doped NWs, which only deliver 0.38 mA/cm² (Figure 5.a and c) even after Co deposition, under the same conditions. Noteworthy, the Co-decorated NW samples featuring the buried p-n junction appear to outperform the recently reported monolithic GaAs NW photocathodes decorated with Pt nanoparticles tested under acidic conditions (pH 1, simulated 1 sun irradiation, 0.87 mA/cm^2 at 0 V vs RHE)[14]. These results demonstrate that the careful tuning of the NW dimensions and structure, combined with non-noble-metal catalysts can provide viable alternatives for the design of efficient photocathodes for HER in neutral electrolyte.

Enhancement of the stability through TiO_2 protection

Despite their promising performances for the photoelectrocatalytic water splitting, III-V SCs suffer from degradation through photocorrosion when placed in aqueous electrolytes. To overcome this issue, an amorphous TiO_2 protective layer of about 5-7 nm thickness was deposited by atomic layer deposition (ALD) on the p-core / n-shell NWs. This deposition technique was chosen to ensure a conformal deposition[22–25]. Scanning transmission electron microscopy (STEM) and electron energy-loss spectroscopy (EELS) were performed on the cross section of a typical NW, as shown in Figure 6. The TiO_2 protective shell is visible in Figure 6.e, which is a higher magnification of the Z-contrast high-angle annular dark field (HAADF) image in Figure 6.a. Ga and Ti EELS elemental maps shown in Figure 6.b (Ga core), Figure 6.c (Ti shell) and Figure 6.d (Ga core + Ti shell) confirm the core-shell geometry of the NWs. Figure 6.e-h, provide a closer view of the 5-7 nm thick protective TiO_2 shell.

LSV measurements performed on p-core/n-shell sample, with and without the protection of the TiO_2 layer and after deposition of the Co nanoparticles are shown in Figure 7.a. Despite the slight

decrease of the current density from about 1.15 mA/cm² down to 0.8 mA/cm² at 0 V vs RHE, which is attributed to the induced resistivity of the oxide layer covering the NWs, the stability of the measured photocurrent over time was enhanced with TiO_2. Indeed, Figure 7.b shows the chronoamperometric (CA) measurements recorded under simulated 1 sun illumination over 13 h. During the first 30 minutes, the sample without the protection layer (purple line) delivered a higher current density compared to the sample with a protective layer (dark blue line). However, after less than one hour, the photocurrent of the sample without TiO_2 shell dropped and stabilized at around 0.06 mA/cm². Meanwhile, the sample with the protective shell stabilized after few hours at around 0.15 mA/cm². These results show that the addition of this protective oxide shell induces a significant enhancement of the stability of the photocathode over time likely due to the reduced photocorrosion of the GaAs NWs. It is worth noting that the transient photocurrents recorded at the start of the chronoamperometry is a common feature observed for photoelectrodes[26–28]. The rapid rise and decay of photocurrent when irradiation is switched on, is mostly representative of non-faradaic processes, like charge accumulation, occurring mostly at the liquid-semiconductor and TiO_2-GaAs interfaces . The distinct interfaces of the samples w/o TiO_2 shell with the electrolyte explain the various transient photocurrents measured.

Importantly, a substantial increase of the Faradaic efficiency (FE) measured for H_2 production is observed for the samples bearing the TiO_2 protective layer, with a yield reaching 59% when unprotected samples yield about 27% FE only. These measurements are limited by the use of single compartmented cell that was necessary to accommodate the samples, allowing for the diffusion of traces of O_2 produced at the anode to the photocathode where O_2 is reduced competitively against protons. The FE values reported here, are thus likely underestimated.

After the reaction, a cross section lamella was extracted from the electrode and characterized using STEM-EELS, as shown in Figure 8.a-d. As expected the TiO_2 shell successfully protected the GaAs core, and remained intact with no distinct degradation, confirming the efficiency of the protection. The improved FE observed for TiO_2-coated samples is, thus, attributed to the reduced photocorrosion of the GaAs semiconductor otherwise leading to an evolution of the chemical composition of the NWs surface likely promoting competitive catalytic or non-catalytic side reactions (O_2 reduction, electrochemical surface etching…).

Conclusions

In this study, the influence of the geometry of GaAs semiconductor as photocathodes for the water reduction was investigated. A strong improvement of the cell efficiency was demonstrated for the 1-dimensional NW geometry, which is mainly due to a significant reduction of light reflected by the electrode. The photoelectrochemical activity was strongly enhanced using the combination of a p-n junction buried within the GaAs NW and of the deposition of Co nanoparticles acting as catalysts for the HER. Furthermore, the stability of the NW-based photocathode over time was significantly improved with the deposition of a thin TiO_2 protective layer, leading to an increase of the efficiency of the cells by a factor 3 after 13 hours. The fabricated photocathodes display photocurrent density up to 1.15 mA/cm² at 0 V vs RHE under neutral conditions. Such performance is at the state of the art for similar GaAs photoelectrodes but would lead to tandem photoelectrochemical cells with solar-to-hydrogen performances below 1%. This calls for future tenfold improvement of the performances of such scalable materials to allow for a viable solar hydrogen technology.

Methods

All the GaAs NWs samples were grown on 2 inches epi-ready p++ Si(111) substrates (Sil'tronix silicon technologies) using a solid-source molecular beam epitaxy (MBE) reactor. The SiO_2 native oxide on the Si substrates was preserved in order to enable the self-assisted growth[29]. The wafers were cleaned in acetone and ethanol during 10 minutes in ultrasonic bath, and were degassed at 200°C under ultra-high vacuum before their introduction inside the MBE chamber. The thin film was synthetized for 20 minutes at a growth rate of about 0.25 nm/s, leading to a thickness of around 300 nm on a 1 x 1 cm^2 Si(111) substrate, leading to a total GaAs volume of around 3.0×10^{-5} cm^3, and an effective surface of 1 cm^2. For the self-assisted GaAs NWs, the substrate was heated to 440°C and 1 monolayer (ML)[30,31] of Ga was pre-deposited to form the Ga catalyst droplet, at a deposition rate of 0.08 ML/s, measured in units of equivalent growth rates of GaAs 2D layers by RHEED oscillations on a GaAs substrate[32]. The sample was then heated to 570°C and the Ga and As_4 fluxes were opened simultaneously to initiate the growth of the self-assisted GaAs NWs. A precise control of the incoming fluxes, valves and shutters was operated via a homemade software. The GaAs NWs were grown with a Ga and As_4 flux of 0.5 ML/s and 1.2 ML/s, respectively, corresponding to a V/III flux ratio of 2.4. The NWs were doped with Be, ensuring the p-doping of the objects. In order to investigate the influence of the NW morphology on the PEC efficiency, the GaAs NWs were radially grown during 1 and 2 hours with a V/III flux ratio of 2.4, at a thermocouple temperature of 400°C. The p-n junction was elaborated with a 1 hour growth of p-doped (Be) core, followed by the growth of the n-doped (Si) shell during 1 hour. All the growths were monitored by RHEED at 20 keV, to obtain information on the crystal structure evolution of the NWs. The samples were rotating all along the growth to ensure the homogeneity of the NWs. Each sample was imaged and characterized with a JEOL SEM using a 10 kV acceleration voltage.

The effective surface of the samples was determined as follows: The surface of a single NW was calculated with an average length of 2.35 µm (2.35×10^{-4} cm) and an average diameter of 125 nm (1.25×10^{-5} cm) giving $S_{NW} = 9.22 \times 10^{-9}$ cm². The NW density (1.1 NW/µm² = 1.1×10^{8} NW/cm²) was finally used to calculate the total effective area $S_{eff} = 1.01$ cm².

The reflectivity measurements were performed with a home-built reflectivity setup. The excitation is a white light (Halogen lamp) that is collimated and focused onto a 200 µm-diameter spot on the sample. The reflected light is collimated and is either i) directly imaged by a CMOS camera for a quick visualization (inset in Figure 3.e), or is ii) projected onto the entrance slit of the spectrometer then collected by a CCD camera at the output of the spectrometer to obtain the reflectivity spectra.

The TiO_2 protective shell was deposited by PE-ALD at 250°C and around 200 mTorr using tetrakis(dimethylamido)titanium (TDMAT) as metal precursor and gaseous O_2 as oxygen precursor.

The degradation of the NWs after the PEC and the homogeneity of the TiO_2 shell deposition were investigated in high-resolution by HAADF-STEM. The chemical study of the GaAs/TiO_2 interface was highlighted by elemental maps using EELS, in STEM mode. The HAADF-STEM and STEM-EELS analyses were performed in a JEOL JEM-ARM200F NeoARM, equipped with a cold-FEG, a last generation aberration-corrector (CEOS ASCOR) of the probe-forming lenses, a Gatan GIF Quantum, and operated at 200 kV. The cross-section lamellae were extracted from the electrode using focused ion beam (FIB) lift-out. STEM-EELS datasets were acquired using the spectrum imaging technique implemented in Gatan microscopy suite. Elemental maps of 158 × 242 pixels were obtained from the Ga-L_{23} and Ti-L_{23} edges, with an exposure times of 5.0 ms and

a dispersion of 1.0 eV/channel. The noise level was minimized by post-processing using principal component analysis implemented in Gatan microscopy suite[33].

All chemicals used for the (photo)electrochemical measurements were obtained from Merck and used as received. The measurements were conducted in the three-electrode configuration using a BioLogic SP300 potentiostat. They were run in a single compartment gas-tight cell in N_2-purged 0.1 M potassium phosphate buffer (pH 7). GaAs samples were used as working electrodes (WE) and mounted on FTO-coated glass (3.1 mm thickness; 7 Ω/cm^{-2}, SOLEMS S.A.) using silver paste to ensure the electrical contact between the back of the GaAs samples and the FTO coating. An O-ring was used to define the active surface area of the electrode material in contact with the electrolyte (geometrical surface area of 0.384 cm^2). A titanium wire was used as counter electrode (CE) and a home-made Ag/AgCl (3 M KCl) electrode as reference electrode (RE). The $[Fe(CN)_6]^{3-}$ /$[Fe(CN)_6]^{4-}$ couple (E = 0.425 V vs NHE in 0.1 M potassium phosphate buffer at pH = 7) was used to standardize the measurements in aqueous solution[34]. Potentials are referred to RHE by using the equation $E_{RHE} = E_{Ag/AgCl} + (E^0_{Ag/AgCl} + 0.059 \times pH)$ where E_{RHE} is the reported potential vs. RHE, $E_{Ag/AgCl}$ the potential measured vs the Ag/AgCl RE, and $E^0_{Ag/AgCl}$ the standard potential of the RE (0.223 V vs NHE)[35]. Co nanoparticles were deposited form a solution of 0.5 mM $Co(NO_3)_2.6H_2O$ in 0.5 M phosphate buffer at pH 7, by applying a potential of −0.65 V vs Ag/AgCl (−0.01 V vs RHE), for 45 minutes under 1 sun simulated irradiation (see below).

Linear sweep voltammetry (LSV) measurements were performed at 10 mV/s scan rate under chopped light irradiation. Photoelectrocatalytic experiments were performed under continuous light irradiation, by running chronoamperometry (CA) measurement at an applied potential of −0.8 V vs Ag/AgCl (−0.18V vs RHE). During the LSV and CA measurements the samples were front-illuminated using a class 3A solar simulator (Newport) equipped with an ozone-free 300 W Xe Arc lamp operated at 280 W and an AM 1.5 G filter. A calibrated reference cell (model 91150V,

Newport) was used to adjust the irradiance at the surface of the sample to 100 mW/cm^2 (simulated 1 sun irradiation). The H_2 accumulated in the headspace during the experiments was quantified by gas chromatography (GC) on a Clarus® 580 gas-chromatograph (PerkinElmer) by direct injection of 50 μL of a sample of the headspace gas, at the end of the CA. A calibration curve was previously established using N_2-H_2 mixtures of known ratio. Before the photoelectrocatalytic measurement, the electrolyte was thoroughly purged with nitrogen gas, until no traces of oxygen could be detected by GC measurements (ca 20 mins). The % Faradaic efficiency was calculated according to the equation: $\eta_F(\%) = [(\text{mols of } H_2 \times 2F)/Q] \times 100$, where F is the Faraday constant (96485 C·mol^{-1}) and Q is the charged passed during the experiment.

Figures

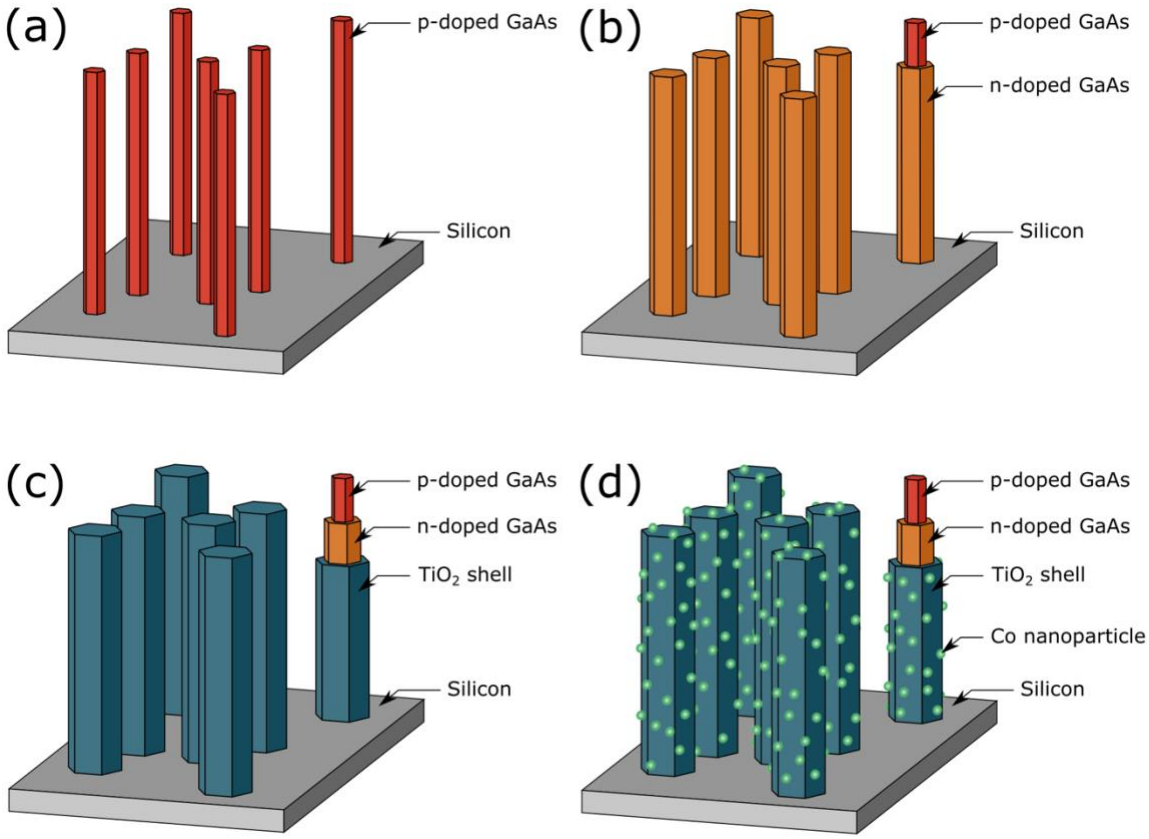

Figure 1. Synthesis steps of the GaAs nanowires. Molecular beam epitaxy growth of p-doped GaAs core (a), n-doped GaAs shell (b), Atomic layer deposition of TiO_2 shell (c), and photoassisted deposition of Co nanoparticles (d).

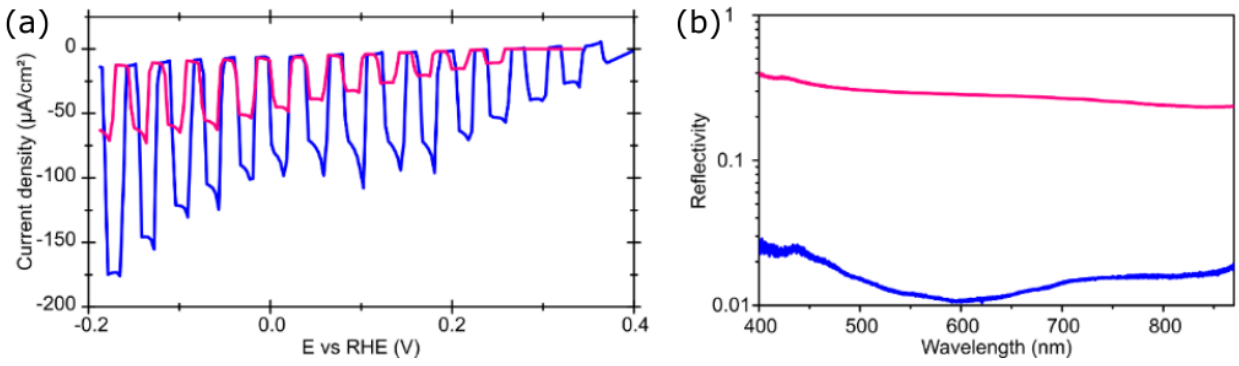

Figure 2. (a) Linear sweep voltammograms (10 mV/s) recorded in nitrogen-saturated 0.1 M potassium phosphate buffer (pH 7), under chopped-light irradiation (simulated 1 sun, 1.5 AM

filter). (b) Reflectivity measured on a 400-870 nm range spectrum. The *y*-axis is in log scale. Pink and blue curves in (a) and (b) correspond to the B-doped GaAs thin film and to the self-assisted B-doped GaAs NWs, respectively.

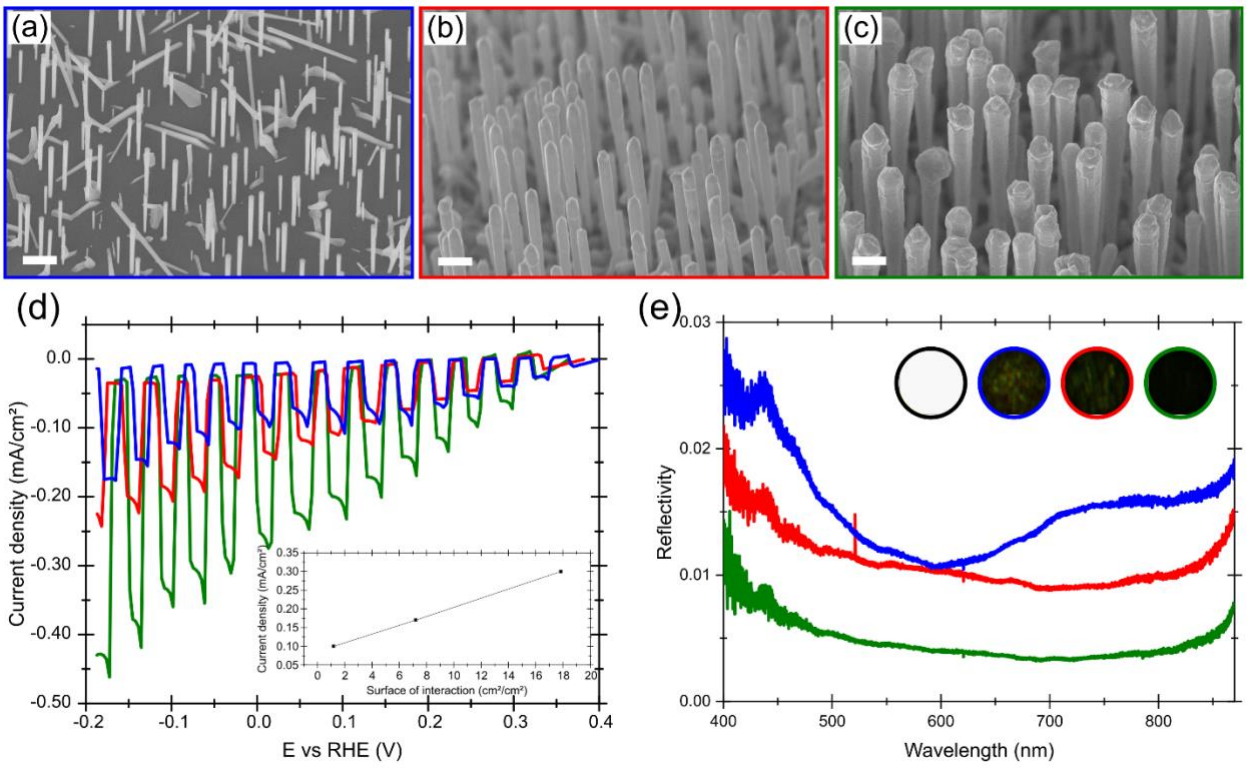

Figure 3. (a) - (c) SEM images of the samples showing the different morphologies obtained for various growth times. Scale bars are 1 µm. (d) PEC characterization of the 3 samples recorded at 10 mV/s in nitrogen saturated 0.1 M potassium phosphate buffer (pH 7), under chopped-light irradiation (1 sun, 1.5 AM filter). (e) Reflectivity of the samples measured on a 400-870 nm range spectrum. Blue, red and green curves displayed in (d) and (e) correspond to the NWs samples showed in (a), (b) and (c), respectively. Inset in (d) represent the current density obtained at 0 V vs RHE as a function of the effective surface of B-doped GaAs materials on 1 cm² of silicon substrate.

Insets in (e) show pictures of the reference mirror (circled in black) and of the samples (a), (b) and (c), circled in blue, red and green, respectively.

Table 1. Measured length and diameter for the samples shown in **Error! Reference source not found.**.a-c, here named as sample 1-3, respectively.

	Sample 1	Sample 2	Sample 3
Length (µm)	2.3 ± 0.3	5.2 ± 0.4	9.4 ± 0.3
Diameter (nm)	125 ± 20	380 ± 20	740 ± 0.4
Density (NWs/µm^2)	1.1	1.0	0.9
Aspect ratio (L/D)	18.4	13.7	12.7
Surface area (cm^2)	1.0	7.2	17.8

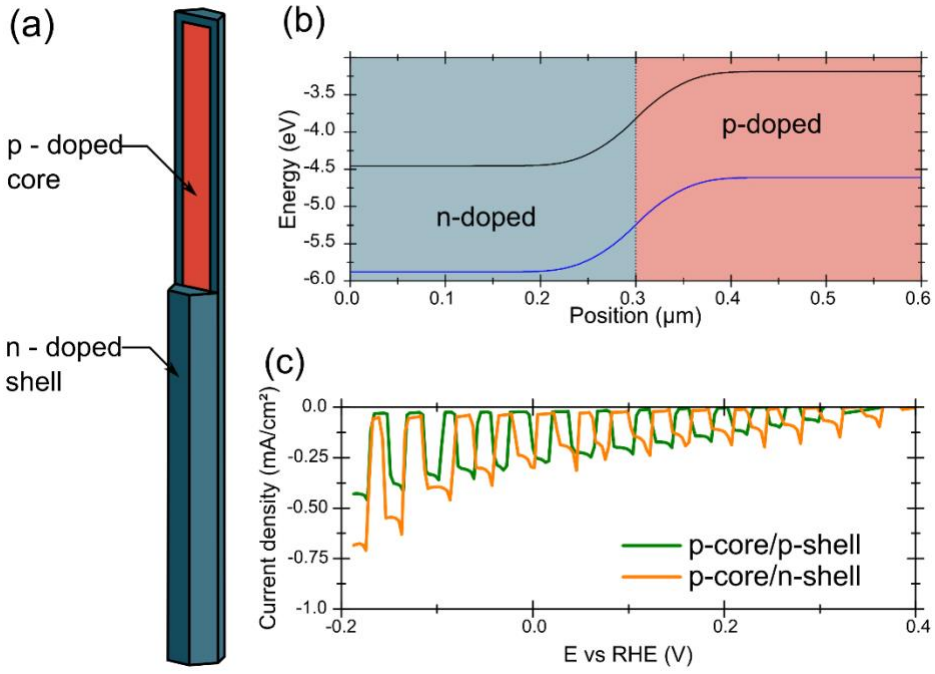

Figure 4. (a) Schematic representation of the core-shell p-n (B-doped GaAs/ Si-doped GaAs) NW structure, showing the p-doped core (orange) and the n-doped shell (blue). (b) Simulation of the

energy band diagram at the interface between the n-doped and the p-doped GaAs. The conduction and the valence bands are represented by the black and blue curves, respectively. (c) LSV measurements performed at 10 mV/s in 0.1 M potassium phosphate buffer (pH 7) under nitrogen, irradiated with chopped light (1 sun, 1.5 AM filter), showing the current densities of a sample without p-n junction (in green) and with p-n junction (in orange).

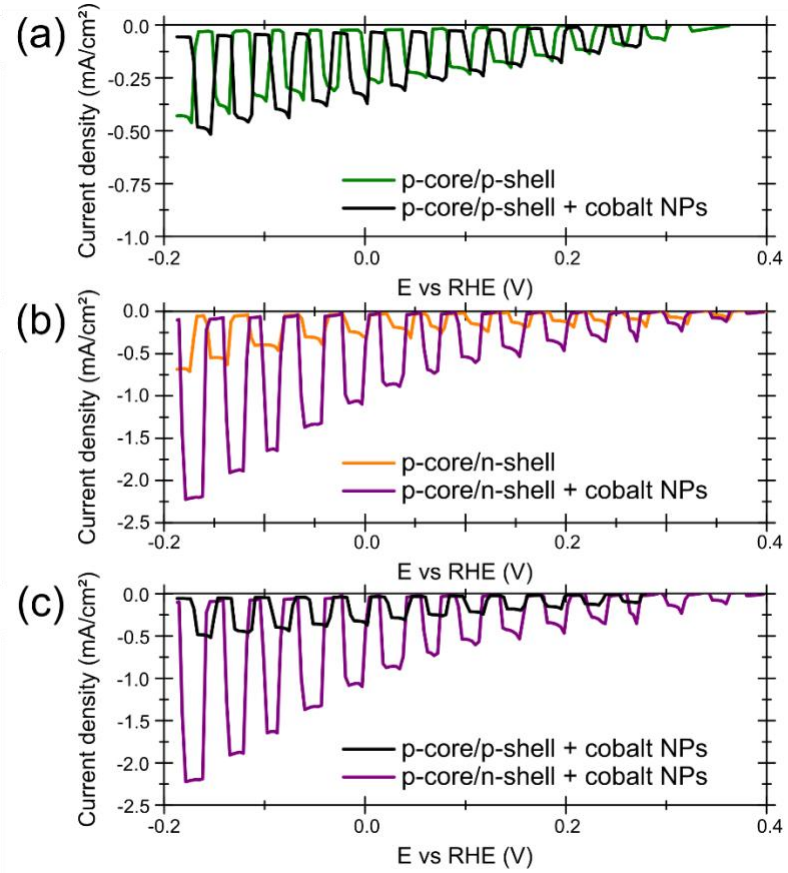

Figure 5. (a)-(c) LSV measurements performed at 10 mV/s in 0.1 M potassium phosphate buffer (pH 7) under nitrogen, irradiated with chopped light (1 sun, 1.5 AM filter), showing the current density of samples with and without p-n junction in orange and green, respectively. The purple and black curves respectively report on the current density obtained for samples with and without p-n

junction, after the deposition of cobalt-catalyst nanoparticles. The cobalt nanoparticles were deposited at -0.65 V vs Ag/AgCl during 45 minutes, under simulated 1 sun illumination.

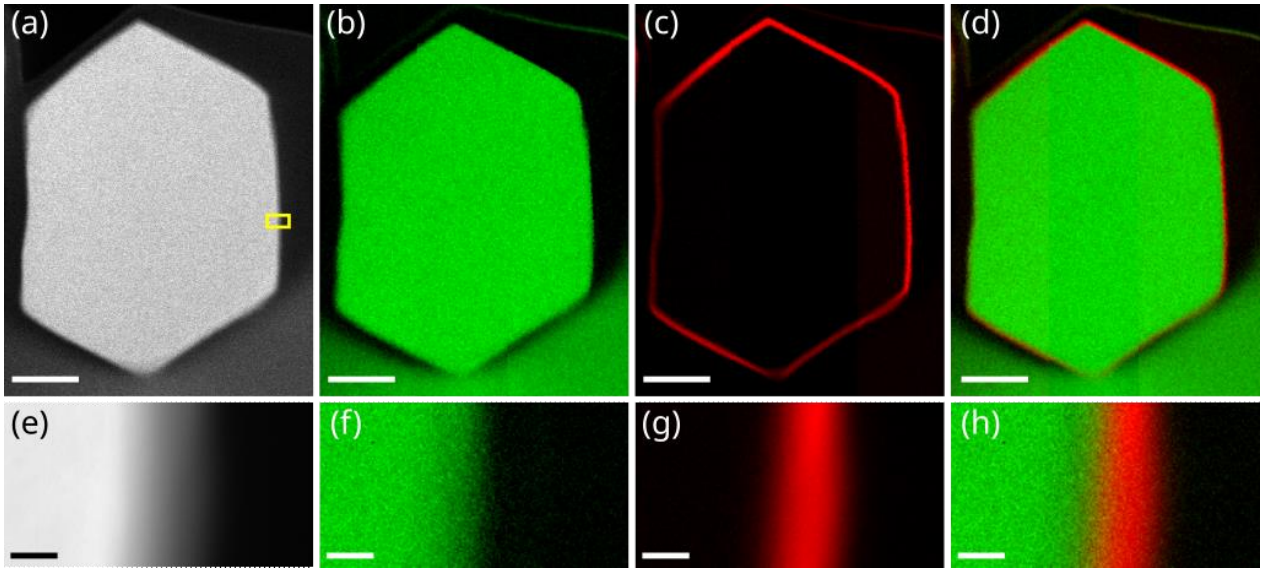

Figure 6. (a) and (e) STEM-HAADF image of the cross-section of a core/shell GaAs NW with a TiO_2 protective shell. (b) and (f) Ga core, (c) and (g) Ti shell. (d) and (h) superimposed EELS maps of the Ga core (green) and Ti shell (red). (e) – (h) maps were obtained from the yellow rectangle in (a). Scale bars in (a)-(d) are 100 nm. Scale bars in (e)-(h) are 5 nm.

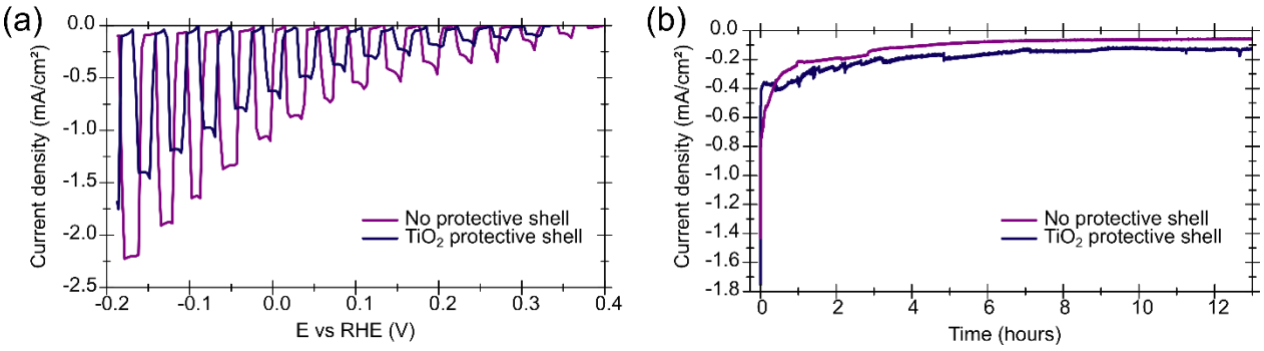

Figure 7. (a) LSV measurements performed at 10 mV/s in 0.1 M potassium phosphate buffer (pH 7) under nitrogen, irradiated with chopped light (1 sun, 1.5 AM filter), showing the current density

of the p-n junction samples, with and without the 10 nm thick TiO_2 protective shell. (b) Chronoamperometric measurements recorded for 13 hours at −0.18 V vs RHE in 0.1 M potassium phosphate buffer (pH 7) under simulated 1 sun illumination for sample with and without TiO_2 protective shell. The dark blue and purple curves on (a) and (b) correspond to the sample with and without the TiO_2 protective shell, respectively.

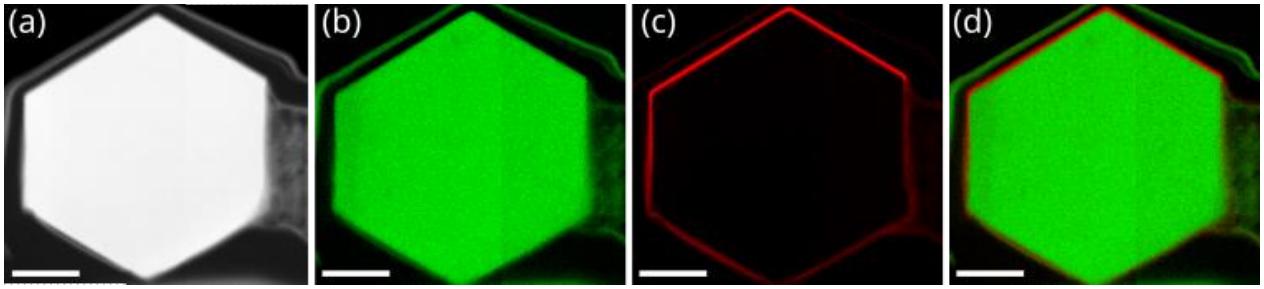

Figure 8. (a) STEM-HAADF image of the cross-section of a GaAs NW with a TiO_2 protective shell after photoelectrocatalysis measurements. Photoelectrocatalytic HER experiments were conducted at -0.18V vs RHE under simulated 1 sun irradiation. (b) Ga core, (c) Ti shell and (d) superimposed EELS maps of the Ga core (green) and Ti shell (red). Scale bars are 100 nm.

Associated content

Supporting information available: Details of the FDTD simulation of the optical properties of the different samples studied, including Figures S1-S3. (DOCX)

Author information

Corresponding Author

*Address correspondence to matthieu.koepf@cea.fr (MK), matthieu.bugnet@insa-lyon.fr (MB), jose.penuelas@ec-lyon.fr (JP)

Acknowledgments

The authors acknowledge access to equipments at the NanoLyon platform and thank J. B. Goure for technical assistance. The authors acknowledge funding from the French Agence Nationale de la Recherche (ANR) for project BEEP 18-CE05-0017-01, Labex ARCANE and CBH-EUR-GS (ANR-17-EURE-0003). The (S)TEM work was performed at the consortium Lyon-St-Etienne de microscopie. The authors are grateful to Y. Lefkir and S. Reynaud for technical assistance using the Jeol NeoARM instrument.

References

(1) Shafiee, S.; Topal, E. An Econometrics View of Worldwide Fossil Fuel Consumption and the Role of US. *Energy Policy* **2008**, *36* (2), 775–786. https://doi.org/10.1016/j.enpol.2007.11.002.

(2) Lewis, N. S. Introduction: Solar Energy Conversion. *Chem. Rev.* **2015**, *115* (23), 12631–12632. https://doi.org/10.1021/acs.chemrev.5b00654.

(3) Detz, R. J.; Reek, J. N. H.; van der Zwaan, B. C. C. The Future of Solar Fuels: When Could They Become Competitive? *Energy Environ. Sci.* **2018**, *11* (7), 1653–1669. https://doi.org/10.1039/C8EE00111A.

(4) Kim, J. H.; Hansora, D.; Sharma, P.; Jang, J.-W.; Lee, J. S. Toward Practical Solar Hydrogen Production – an Artificial Photosynthetic Leaf-to-Farm Challenge. *Chem. Soc. Rev.* **2019**, *48* (7), 1908–1971. https://doi.org/10.1039/C8CS00699G.

(5) Walter, M. G.; Warren, E. L.; McKone, J. R.; Boettcher, S. W.; Mi, Q.; Santori, E. A.; Lewis, N. S. Solar Water Splitting Cells. *Chem. Rev.* **2010**, *110* (11), 6446–6473. https://doi.org/10.1021/cr1002326.

(6) Fujishima, A.; Honda, K. Electrochemical Photolysis of Water at a Semiconductor Electrode. *Nature* **1972**, *238* (5358), 37–38. https://doi.org/10.1038/238037a0.

(7) Ni, M.; Leung, M. K. H.; Leung, D. Y. C.; Sumathy, K. A Review and Recent Developments in Photocatalytic Water-Splitting Using TiO2 for Hydrogen Production. *Renewable and Sustainable Energy Reviews* **2007**, *11* (3), 401–425. https://doi.org/10.1016/j.rser.2005.01.009.

(8) Sivula, K.; van de Krol, R. Semiconducting Materials for Photoelectrochemical Energy Conversion. *Nat Rev Mater* **2016**, *1* (2), 15010. https://doi.org/10.1038/natrevmats.2015.10.

(9) Standing, A.; Assali, S.; Gao, L.; Verheijen, M. A.; van Dam, D.; Cui, Y.; Notten, P. H. L.; Haverkort, J. E. M.; Bakkers, E. P. A. M. Efficient Water Reduction with Gallium Phosphide Nanowires. *Nat Commun* **2015**, *6* (1), 7824. https://doi.org/10.1038/ncomms8824.

(10) Alqahtani, M.; Ben-Jabar, S.; Ebaid, M.; Sathasivam, S.; Jurczak, P.; Xia, X.; Alromaeh, A.; Blackman, C.; Qin, Y.; Zhang, B.; Ooi, B. S.; Liu, H.; Parkin, I. P.; Wu, J. Gallium Phosphide Photoanode Coated with TiO_2 and CoO_X for Stable Photoelectrochemical Water Oxidation. *Opt. Express* **2019**, *27* (8), A364. https://doi.org/10.1364/OE.27.00A364.

(11) Wang, S.; Liu, G.; Wang, L. Crystal Facet Engineering of Photoelectrodes for Photoelectrochemical Water Splitting. *Chem. Rev.* **2019**, *119* (8), 5192–5247. https://doi.org/10.1021/acs.chemrev.8b00584.

(12) Deng, J.; Su, Y.; Liu, D.; Yang, P.; Liu, B.; Liu, C. Nanowire Photoelectrochemistry. *Chem. Rev.* **2019**, *119* (15), 9221–9259. https://doi.org/10.1021/acs.chemrev.9b00232.
(13) Kornienko, N.; Gibson, N. A.; Zhang, H.; Eaton, S. W.; Yu, Y.; Aloni, S.; Leone, S. R.; Yang, P. Growth and Photoelectrochemical Energy Conversion of Wurtzite Indium Phosphide Nanowire Arrays. *ACS Nano* **2016**, *10* (5), 5525–5535. https://doi.org/10.1021/acsnano.6b02083.
(14) Cui, F.; Zhang, Y.; Fonseka, H. A.; Promdet, P.; Channa, A. I.; Wang, M.; Xia, X.; Sathasivam, S.; Liu, H.; Parkin, I. P.; Yang, H.; Li, T.; Choy, K.-L.; Wu, J.; Blackman, C.; Sanchez, A. M.; Liu, H. Robust Protection of III–V Nanowires in Water Splitting by a Thin Compact TiO $_2$ Layer. *ACS Appl. Mater. Interfaces* **2021**, *13* (26), 30950–30958. https://doi.org/10.1021/acsami.1c03903.
(15) Zhou, P.; Navid, I. A.; Ma, Y.; Xiao, Y.; Wang, P.; Ye, Z.; Zhou, B.; Sun, K.; Mi, Z. Solar-to-Hydrogen Efficiency of More than 9% in Photocatalytic Water Splitting. *Nature* **2023**, *613* (7942), 66–70. https://doi.org/10.1038/s41586-022-05399-1.
(16) Segev, G.; Kibsgaard, J.; Hahn, C.; Xu, Z. J.; Cheng, W.-H. (Sophia); Deutsch, T. G.; Xiang, C.; Zhang, J. Z.; Hammarström, L.; Nocera, D. G.; Weber, A. Z.; Agbo, P.; Hisatomi, T.; Osterloh, F. E.; Domen, K.; Abdi, F. F.; Haussener, S.; Miller, D. J.; Ardo, S.; McIntyre, P. C.; Hannappel, T.; Hu, S.; Atwater, H.; Gregoire, J. M.; Ertem, M. Z.; Sharp, I. D.; Choi, K.-S.; Lee, J. S.; Ishitani, O.; Ager, J. W.; Prabhakar, R. R.; Bell, A. T.; Boettcher, S. W.; Vincent, K.; Takanabe, K.; Artero, V.; Napier, R.; Cuenya, B. R.; Koper, M. T. M.; Van De Krol, R.; Houle, F. The 2022 Solar Fuels Roadmap. *J. Phys. D: Appl. Phys.* **2022**, *55* (32), 323003. https://doi.org/10.1088/1361-6463/ac6f97.
(17) Deng, J.; Su, Y.; Liu, D.; Yang, P.; Liu, B.; Liu, C. Nanowire Photoelectrochemistry. *Chemical Reviews* **2019**, *119* (15), 9221–9259. https://doi.org/10.1021/acs.chemrev.9b00232.
(18) Lee, M. H.; Takei, K.; Zhang, J.; Kapadia, R.; Zheng, M.; Chen, Y.-Z.; Nah, J.; Matthews, T. S.; Chueh, Y.-L.; Ager, J. W.; Javey, A. P-Type InP Nanopillar Photocathodes for Efficient Solar-Driven Hydrogen Production. *Angew. Chem. Int. Ed.* **2012**, *51* (43), 10760–10764. https://doi.org/10.1002/anie.201203174.
(19) Standing, A.; Assali, S.; Gao, L.; Verheijen, M. A.; van Dam, D.; Cui, Y.; Notten, P. H. L.; Haverkort, J. E. M.; Bakkers, E. P. A. M. Efficient Water Reduction with Gallium Phosphide Nanowires. *Nat Commun* **2015**, *6* (1), 7824. https://doi.org/10.1038/ncomms8824.
(20) Piriyev, M.; Loget, G.; Léger, Y.; Chen, L.; Létoublon, A.; Rohel, T.; Levallois, C.; Le Pouliquen, J.; Fabre, B.; Bertru, N.; Cornet, C. Dual Bandgap Operation of a GaAs/Si Photoelectrode. *Solar Energy Materials and Solar Cells* **2023**, *251*, 112138. https://doi.org/10.1016/j.solmat.2022.112138.
(21) Cobo, S.; Heidkamp, J.; Jacques, P.-A.; Fize, J.; Fourmond, V.; Guetaz, L.; Jousselme, B.; Ivanova, V.; Dau, H.; Palacin, S.; Fontecave, M.; Artero, V. A Janus Cobalt-Based Catalytic Material for Electro-Splitting of Water. *Nature Mater* **2012**, *11* (9), 802–807. https://doi.org/10.1038/nmat3385.
(22) Chandrasekaran, S.; Kaeffer, N.; Cagnon, L.; Aldakov, D.; Fize, J.; Nonglaton, G.; Baleras, F.; Mailley, P.; Artero, V. A Robust ALD-Protected Silicon-Based Hybrid Photoelectrode for Hydrogen Evolution under Aqueous Conditions. *Chem. Sci.* **2019**, *10* (16), 4469–4475. https://doi.org/10.1039/C8SC05006F.
(23) Gu, J.; Yan, Y.; Young, J. L.; Steirer, K. X.; Neale, N. R.; Turner, J. A. Water Reduction by a P-GaInP2 Photoelectrode Stabilized by an Amorphous TiO2 Coating and a Molecular Cobalt Catalyst. *Nature Mater* **2016**, *15* (4), 456–460. https://doi.org/10.1038/nmat4511.

(24) Hu, S.; Shaner, M. R.; Beardslee, J. A.; Lichterman, M.; Brunschwig, B. S.; Lewis, N. S. Amorphous TiO 2 Coatings Stabilize Si, GaAs, and GaP Photoanodes for Efficient Water Oxidation. *Science* **2014**, *344* (6187), 1005–1009. https://doi.org/10.1126/science.1251428.
(25) Moehl, T.; Suh, J.; Sévery, L.; Wick-Joliat, R.; Tilley, S. D. Investigation of (Leaky) ALD TiO 2 Protection Layers for Water-Splitting Photoelectrodes. *ACS Appl. Mater. Interfaces* **2017**, *9* (50), 43614–43622. https://doi.org/10.1021/acsami.7b12564.
(26) Dumortier, M.; Bosserez, T.; Rongé, J.; Martens, J. A.; Haussener, S. Combined Experimental-Numerical Analysis of Transient Phenomena in a Photoelectrochemical Water Splitting Cell. *The Journal of Physical Chemistry C* **2016**, *120* (7), 3705–3714. https://doi.org/10.1021/acs.jpcc.5b12445.
(27) Laskowski, F. A. L.; Qiu, J.; Nellist, M. R.; Oener, S. Z.; Gordon, A. M.; Boettcher, S. W. Transient Photocurrents on Catalyst-Modified N-Si Photoelectrodes: Insight from Dual-Working Electrode Photoelectrochemistry. *Sustainable Energy & Fuels* **2018**, *2* (9), 1995–2005. https://doi.org/10.1039/C8SE00187A.
(28) Le Formal, F.; Sivula, K.; Grätzel, M. The Transient Photocurrent and Photovoltage Behavior of a Hematite Photoanode under Working Conditions and the Influence of Surface Treatments. *The Journal of Physical Chemistry C* **2012**, *116* (51), 26707–26720. https://doi.org/10.1021/jp308591k.
(29) Fontcuberta i Morral, A.; Spirkoska, D.; Arbiol, J.; Heigoldt, M.; Morante, J. R.; Abstreiter, G. Prismatic Quantum Heterostructures Synthesized on Molecular-Beam Epitaxy GaAs Nanowires. *Small* **2008**, *4* (7), 899–903. https://doi.org/10.1002/smll.200701091.
(30) Küpers, H.; Bastiman, F.; Luna, E.; Somaschini, C.; Geelhaar, L. Ga Predeposition for the Ga-Assisted Growth of GaAs Nanowire Ensembles with Low Number Density and Homogeneous Length. *Journal of Crystal Growth* **2017**, *459*, 43–49. https://doi.org/10.1016/j.jcrysgro.2016.11.065.
(31) Fouquat, L.; Vettori, M.; Botella, C.; Benamrouche, A.; Penuelas, J.; Grenet, G. X-Ray Photoelectron Spectroscopy Study of Ga Nanodroplet on Silica-Terminated Silicon Surface for Nanowire Growth. *Journal of Crystal Growth* **2019**, *514*, 83–88. https://doi.org/10.1016/j.jcrysgro.2019.03.003.
(32) Rudolph, D.; Hertenberger, S.; Bolte, S.; Paosangthong, W.; Spirkoska, D.; Döblinger, M.; Bichler, M.; Finley, J. J.; Abstreiter, G.; Koblmüller, G. Direct Observation of a Noncatalytic Growth Regime for GaAs Nanowires. *Nano Lett.* **2011**, *11* (9), 3848–3854. https://doi.org/10.1021/nl2019382.
(33) Lucas, G.; Burdet, P.; Cantoni, M.; Hébert, C. Multivariate Statistical Analysis as a Tool for the Segmentation of 3D Spectral Data. *Micron* **2013**, *52–53*, 49–56. https://doi.org/10.1016/j.micron.2013.08.005.
(34) O'Reilly, J. E. Oxidation-Reduction Potential of the Ferro-Ferricyanide System in Buffer Solutions. *Biochimica et Biophysica Acta (BBA) - Bioenergetics* **1973**, *292* (3), 509–515. https://doi.org/10.1016/0005-2728(73)90001-7.
(35) ANALYTICAL CHEMISTRY DIVISION COMMISSION ON ELECTROANALYTICAL CHEMISTRY. In *Classification and Nomenclature of Electroanalytical Techniques*; Elsevier, 1976; pp 83–95. https://doi.org/10.1016/B978-0-08-021226-5.50002-2.

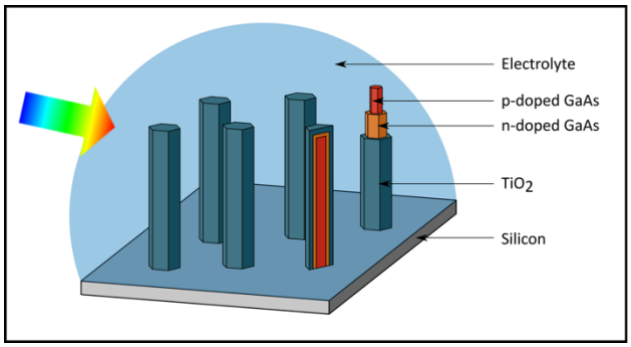
Electrolyte
p-doped GaAs
n-doped GaAs
TiO_2
Silicon